THE EFFECT OF THE ELECTRON DONOR H_3^+ ON THE PRE–MAIN-SEQUENCE AND MAIN-SEQUENCE EVOLUTION OF LOW-MASS, ZERO-METALLICITY STARS

G. J. Harris, A. E. Lynas-Gray,[1] S. Miller, and J. Tennyson

Department of Physics and Astronomy, University College London, London WC1E 6BT, UK; j.tennyson@ucl.ac.uk

ABSTRACT

H_3^+ has been shown (1991 work of Lenzuni and coworkers) to be the dominant positive ion in a zero-metallicity gas at low temperature and intermediate to high density. It therefore affects both the number of free electrons and the opacity of the gas. The most recent H_3^+ partition function (1995 work of Neale & Tennyson) is an order of magnitude larger at 4000 K than all previous partition functions, implying that H_3^+ is a more important electron donor than previously thought. Here we present new Rosseland mean opacities for a hydrogen-helium gas of $1000 \text{ K} \leq T \leq 9000 \text{ K}$ and $-14 \leq \log_{10}[\rho \text{ (g cm}^{-3})] \leq -2$. In the calculation of these opacities, we have made use of the latest collision-induced absorption data as well as the most recent H_3^+ partition function and line opacity data. It is shown that these updated and new sources of opacity give rise to a Rosseland mean opacity for a hydrogen-helium gas that is, in general, greater than that calculated in earlier works. The new opacity data are then used to model the evolution of low-mass (0.15–$0.8 \ M_\odot$), zero-metallicity stars, from pre–main-sequence collapse to main-sequence turnoff. To investigate the effect of H_3^+ on the evolution of low-mass, zero-metallicity stars, we repeat our calculations neglecting H_3^+ as a source of electrons and line opacity. We find that H_3^+ can have an effect on the structure and evolution of stars of mass $\sim 0.5 \ M_\odot$ or less. A gray atmosphere is used for the calculation, which is sufficient to demonstrate that H_3^+ affects the evolution of very low mass stars to a greater degree than previously believed.

Subject headings: atomic data — stars: evolution — stars: low-mass, brown dwarfs

On-line material: machine-readable table

1. INTRODUCTION

It has long been speculated that zero-metallicity Population III stars exist, but as yet none of these stars have been identified. At the current epoch, low-mass stars are the most numerous stars in the Galaxy; however, the first stars are often thought to have formed with exclusively high masses. For example, Tohline (1980) estimated the minimum mass of a Population III star to be a massive 1500 $M_\odot$; more recently, de Araújo & Opher (1989) estimated the minimum mass to be 50 $M_\odot$. On the other hand, Kashlinsky & Rees (1983) proposed a method by which stars of mass as low as 0.2 $M_\odot$ could be formed from primordial material. Recently, using hydrodynamic simulations, Nakamura & Umemura (2001) suggested a bimodal Population III initial mass function with a minimum mass of between 1 and 2 $M_\odot$. The discovery of the extremely metal deficient star HE 0107−5240 (Christlieb et al. 2002), which has an estimated mass of 0.8 $M_\odot$ and $[\text{Fe/H}] = -5.3$, has added credence to the possibility that low-mass primordial stars were formed. All Population III stars with mass less than about 0.75 $M_\odot$ should still be on the main sequence and thus could, if ever observed, provide an estimate of the age of the universe.

The accuracy of stellar formation and evolution calculations is, among other things, dependent on available opacity data. In the absence of metals, the only contributors to the opacity of the atmospheres of Population III stars are the various hydrogen and helium species and ions and electrons. In a zero-metallicity gas at densities common to stellar atmospheres, it is H^- that dominates the opacity at temperatures

between about 3500 and 7000 K. Below about 3500 K, it is collision-induced absorption (CIA) by H_2-He and H_2-H_2 that dominates the opacity. Many authors (Lenzuni, Chernoff, & Salpeter 1991; Alexander & Ferguson 1994; Saumon et al. 1994; Rohrmann 2001; Allard et al. 2001) have commented on how H_3^+ can act as an electron donor in low-metallicity stars, thereby increasing the abundance of H^- and hence the opacity. However, none have yet investigated the effect of H_3^+ rotation-vibration line absorption on a hydrogen-helium gas opacity.

The zero-metallicity opacity calculations of Lenzuni et al. (1991) used the H_3^+ partition function of Patch (1968), whereas the opacity calculations of Alexander & Ferguson (1994), Saumon et al. (1994), and Bergeron, Saumon, & Wesemael (1995) used the partition functions of Chandra, Gaur, & Pande (1991). The partition functions of Patch (1968) and Chandra et al. (1991) are an order of magnitude smaller at $T \sim 4000$ K than the latest, most accurate H_3^+ partition function of Neale & Tennyson (1995). The Neale & Tennyson (1995) H_3^+ partition function was computed by direct summation of 200,000 rotation-vibration energy levels. This most recent H_3^+ partition function has been used extensively in the modeling of cool, stellar, white and brown dwarf atmospheres (Bergeron, Ruiz, & Leggett 1997; Hauschildt, Allard, & Baron 1999; Saumon & Jacobson 1999; Rohrmann 2001; Allard et al. 2001). The cool stellar and brown dwarf atmospheres of Hauschildt et al. (1999) have subsequently been incorporated in evolution models of brown dwarfs and low-mass stars by Chabrier & Baraffe (1997) and Baraffe et al. (1997, 1998, 2002). In particular, Baraffe et al. (1997, 1998) studied very low mass, low-metallicity stars of $[M/H] \geq -2.0$, and Saumon et al. (1994) studied zero-metallicity, very low mass stars with the Chandra et al. (1991) partition function. However, neither the

[1] Permanent address: Department of Physics, University of Oxford, Keble Road, Oxford OX1 3RH, UK.

H_3^+ partition function of Neale & Tennyson (1995) nor any H_3^+ line list has been used in evolution calculations of low-mass, zero- or very low metallicity stars. Recent very low and zero-metallicity, low-mass stellar evolution calculations by Vanden-Berg et al. (2000), Marigo et al. (2001), and Siess, Livio, & Lattanzio (2002) use the low-temperature ($T < 10,000$ K) Alexander & Ferguson (1994) opacities, whereas Richard et al. (2002) use low-temperature opacities based on Kurucz data (see Turcotte et al. 1998; Proffitt 1994). The minimum mass to which these very low metallicity evolution calculations extend is $0.5 \, M_\odot$. As we show below, zero-metallicity stars of mass less than about $0.5 \, M_\odot$ are affected by H_3^+ acting as an electron donor.

In this paper we present new low-temperature Rosseland mean opacities for a zero-metallicity gas in LTE. These opacities have been calculated both with and without the Neale & Tennyson (1995) partition function and the Neale, Miller, & Tennyson (1996) H_3^+ line list. We then incorporate these new opacity data within the CESAM stellar evolution code (Morel 1997) and examine the effect of H_3^+ on the pre–main-sequence and main-sequence evolution of zero-metallicity stars.

2. LOW-TEMPERATURE OPACITY

For compatibility with the CESAM stellar evolution code (Morel 1997), the Rosseland mean opacity must be determined from the state variables of temperature (T), mass density (ρ), and hydrogen mass fraction (X). The opacity of a gas is dependent on its chemical composition, so the abundances of all the species within the gas or plasma must first be determined. For this purpose, thermodynamic and chemical equilibrium are assumed, which for low densities allows the use of the Saha equation to determine the number densities of individual species. By combining these number densities with the cross sections of the relevant scattering or absorption process, we can obtain the total opacity for the process in the gas. Rosseland mean opacities are then computed as below.

2.1. *The Equation of State*

The species that are considered in this work are listed in Table 1 together with the source of the rotational-vibrational partition function if relevant. We use an iterative approach to solve for chemical equilibrium using the Saha equations for each chemical species.

TABLE 1
Species used in the Calculation

Species	T Range (K)	Reference
H_2	1000–9000	1
H...................	...	...
H^-	...	...
H^+	...	...
H_2^+	1500–18000	2
H_2^-	1000–9000	1
H_3^+	500–8000	3
He..................	...	...
He^+	...	...
HeH^+	1000–9000	1
e^-..................	...	...

Note.—The source and the temperature range of the rotational-vibrational partition functions are quoted where applicable.
References.—(1) Sauval & Tatum 1984; (2) Stancil 1994; (3) Neale & Tennyson 1995.

For the initial conditions of our calculation, a neutral H_2 and He gas is used, and the number densities of all other species are set to zero. The initial number densities of H_2 and He are determined from T, ρ, and X. For most of the values of T and ρ considered in this work, H_2, H, and He are the most abundant species. Therefore, we first determine the dominant hydrogen species by calculating a first-order number density of H from H_2 using the Saha equation:

$$\frac{n(H_2)}{n(H)^2} = \frac{Q_T(H_2)}{Q_T(H)^2} \exp\left(\frac{\chi(H_2)}{kT}\right), \qquad (1)$$

where $n(x)$ is the number density of the species x, $Q_T(x)$ is the total partition function of species x, and $\chi(H_2)$ is the dissociation energy of H_2. The total partition function is $Q_T(x)$, which for H_2 is the product of translational, rotational-vibrational, and electronic partition functions. In this work we neglect electronic states higher than the ground state and set the electronic partition function equal to the degeneracy of the ground electronic state.

Equation (1) is solved iteratively, using a Newton-Raphson technique and forcing the conservation of H nuclei. Using the Saha ionization equation, we then determine the first-order number densities of H^+, H^-, He^+, H_2^+, H_2^-, HeH^+, and e^-. Again, an iterative Newton-Raphson technique is employed, taking care to conserve charge and hydrogen and helium nuclei.

The determination of the number density of H_3^+ is slightly more difficult. The usual formation reaction of H_3^+ in the interstellar medium is

$$H_2^+ + H_2 \rightleftharpoons H_3^+ + H \qquad (2)$$

(see, for example, Herbst 2000). In chemical equilibrium, the number density of H_2^+ is often many orders of magnitude smaller than that of H_3^+, which in turn is many orders of magnitude smaller than the number densities of H_2 and H. This can result in problems with machine accuracy. Instead, we estimate the number density of H_3^+ from H_2 or H, depending on whether H_2 or H is more abundant. For instance, if H_2 is dominant, then we use the hypothetical reaction $2H_2 \rightleftharpoons H_3^+ + H + e^-$. This reaction has the Saha equation

$$\frac{n(H_2)^2}{n(H_3^+)n(H)n(e^-)} = \frac{[Q_T(H_2)]^2}{Q_T(H_3^+)Q_T(H)Q_T(e^-)} \exp\left(\frac{\chi}{kT}\right), \quad (3)$$

where χ is the difference in energy between products and reactants. This is equal to the dissociation energy of H_2 (4.52 eV) plus the ionization potential of H (13.60 eV) minus the proton affinity of H_2 (4.38 eV), so $\chi = 13.74$ eV. This approach increases the stability of the calculation of the number density of H_3^+. It is valid because, by definition, in chemical equilibrium each species is in equilibrium with every other species.

Once the first estimate for the number density of H_3^+ has been obtained, the process is reiterated, using the new number densities, until converged values for the number density of each species are obtained.

Figure 1 shows an illustration of the temperature dependences of the number densities of each species at $\rho = 10^{-6}$ g cm^{-3} and $X = 0.72$. Importantly, at $\rho = 10^{-6}$ g cm^{-3}, H_3^+ is the dominant positive ion below 3500 K, so it will have a strong effect on the abundances of ions and electrons below this
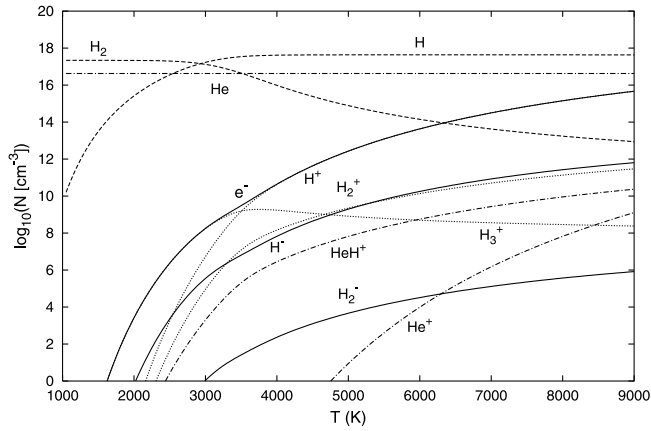
Fig. 1.—Number densities of the species considered in the calculation as a function of temperature, at $\rho = 10^{-6}$ g cm^{-3}. The solid curves represent negatively charged species, the dotted curves represent positively charged hydrogen species, the dashed curves represent neutral hydrogen species, and the dot-dashed curves represent helium-containing species.

Fig. 3.—Number densities of H$_3^+$ and H$^-$ as a function of temperature, at $\rho = 10^{-6}$ g cm^{-3}. The three curves were calculated with the H$_3^+$ partition functions of Neale & Tennyson (1995; *solid curves*), Chandra et al. (1991; *dashed curves*), and Patch (1968; *dotted curves*).

temperature. Figure 2 shows an illustration of the mass-density dependences of the number densities of each species at $T = 3500$ and $X = 0.72$. Here H$_3^+$ becomes the dominant ion above $\rho \sim 2 \times 10^{-6}$. Figure 3 shows the number density of H$^-$ and H$_3^+$ calculated using the H$_3^+$ rotational-vibrational partition functions of Neale & Tennyson (1995), Chandra et al. (1991), and Patch (1968) as a function of temperature with $\rho = 10^{-6}$ and $X = 0.72$. Clearly, the number densities of H$_3^+$ and H$^-$ are strongly dependent on which partition function is used; indeed, above 4000 K use of the Neale & Tennyson (1995) partition function yields an order of magnitude more H$_3^+$ than the use of other partition functions. However, at this mass density H$^+$ becomes the dominant ion above 3700 K, and the effect of H$_3^+$ on H$^-$ quickly diminishes with increasing temperature. Since H$^-$ is an important source of opacity, the opacity is sensitive to which partition function is used in the calculation.

The limits of the partition functions used in this work effectively determine the temperature limits for which this equation of state is reliable. For all but H$_3^+$, the partition
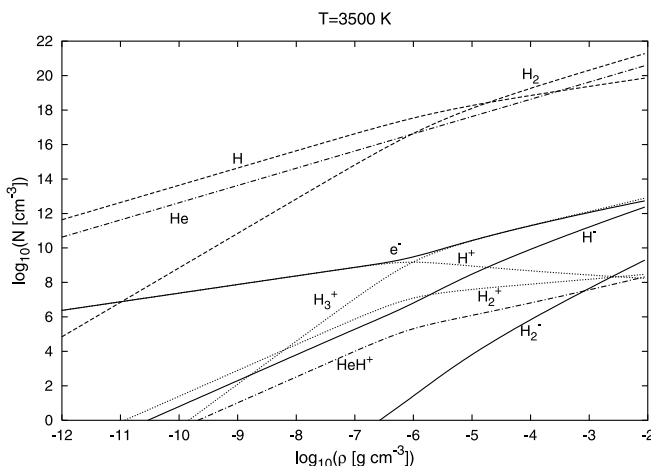

Fig. 2.—Number densities of the species considered in the calculation as a function of density, at $T = 3500$ K. The solid curves represent negatively charged species, the dotted curves represent positively charged hydrogen species, the dashed curves represent neutral hydrogen species, and the dot-dashed curves represent helium-containing species.
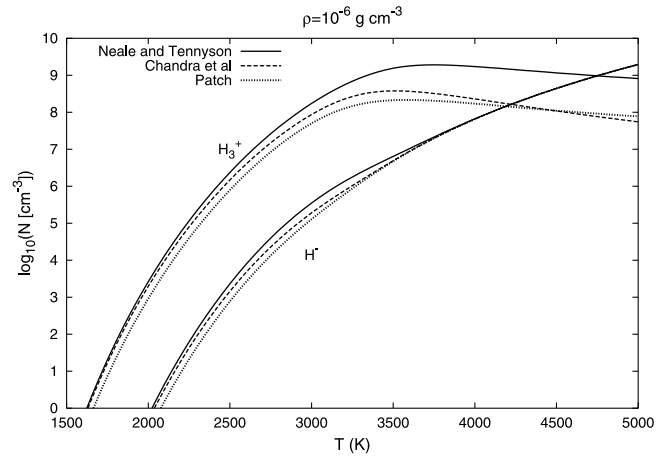
functions extend up to at least 9000 K and down to 1000 K. For H$_3^+$ the Neale & Tennyson (1995) partition function extends to 8000 K. At the densities of interest to us, H$_3^+$ is relatively unimportant between 8000 and 9000 K. Therefore, our equation of state is reliable between 1000 and 9000 K. The main shortcoming of the Saha equation is that it does not account for pressure ionization, which occurs at very high densities. This imposes an upper density limit above which our equation of state is not valid. Mihalas, Däppen, & Hummer (1988) show that for $T < 10,000$ K, the upper density for which the Saha equation is valid is around $\log \rho = -2$. We take this as the upper density limit for our equation of state.

2.1.1. *The Effect of Metals on the Number Density of* H$_3^+$

H$_3^+$ is readily destroyed in a dissociative recombination reaction with electrons. Hence, high abundances of electrons act to reduce the abundance of H$_3^+$. Many species of metals have an ionization energy that is significantly lower than that of hydrogen, so in a gas containing metals, it is the metals that govern the abundance of free electrons. In this way, metals have a strong effect on the abundance of H$_3^+$. Since all known stars contain some metals, we briefly investigate the effect that these metals have on H$_3^+$.

The equation of state is dependent on the relative abundance of each metal. Since the stars in which H$_3^+$ is an important electron donor are likely to be metal-poor, we use the metal abundance mix found in the very metal poor star HE 0107−5240, discovered by Christlieb et al. (2002). Where the abundances of these metals are unmeasured for HE 0107−5240, we use metal abundances based on a theoretical Population III supernova yield calculated by Umeda & Nomoto (2003). In our equation of state we include what are likely to be the 10 most abundant metals in HE 0107−5240: C, N, O, Ne, Na, Mg, Si, S, Ca, and Fe. We included the first ionization states and the anions of the metals within our equation of state.

Figure 4 shows the number densities of H$_3^+$, H$^+$, e^-, and the positive metal ions (Z^+) as a function of temperature, at a density of 10^{-6} g cm^{-3}. From this figure, H$_3^+$ is the dominant positive ion in a gas between temperatures of 3000 and 3600 K, with elemental abundances similar to HE 0107−5240. Figure 5 shows the number densities of H$_3^+$, H$^+$, e^-, and the
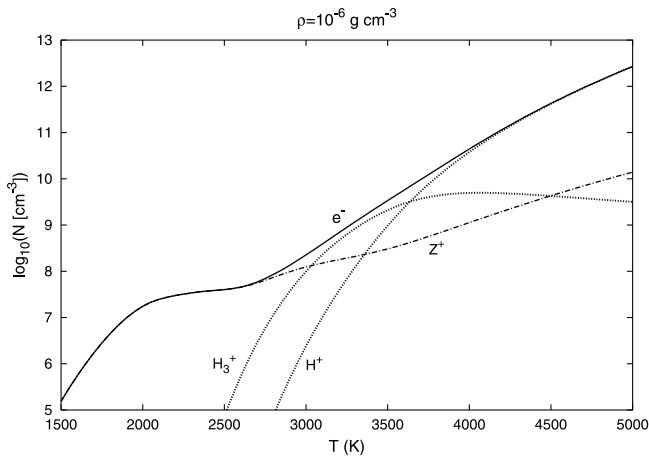
FIG. 4.—Number densities of H_3^+, H^+, e^-, and ionized metals (Z^+) as a function of temperature, at $\rho = 10^{-6}$ g cm^{-3}.

positive metal ions (Z^+) as a function of metal mass fraction. We have used the same metal mix as for Figure 4 with a constant hydrogen mass fraction of $X = 0.72$ and a density of 10^{-6} g cm^{-3}. The total number density of the positive metal ions only exceeds the number density of H_3^+ for metal mass fractions above 10^{-3}. It should be noted that the metal mix found in HE 0107$-$5240 has a very high carbon-to-iron ratio relative to solar ([C/Fe] = 4.0) but has a comparatively low abundance of more readily ionized elements such as Na ([Na/Fe] = 0.8) and Fe. Hence, this metal mix will result in fewer free electrons at low temperatures than a solar metal mix. For a solar metal mix (Grevesse & Sauval 1998) with the same temperature and density, we find that the metals are the main electron donors for metal mass fractions above about 10^{-6}. The relative importance of H_3^+ as an electron donor is not only dependent on metallicity but also on the relative abundances of the metals within the mix.

Density also has a role in determining the dominant positive ion; high densities favor H_3^+, and low densities favor the metal ions. Hence, H_3^+ is more likely to have an effect on very metal poor, low-mass dwarf stars than on low-mass giants.

2.2. The Opacity

The frequency-dependent continuous opacity can now be calculated using the number densities of the various species. In this work the set of subroutines developed by A. J. Booth & A. E. Lynas-Gray (2002, private communication) was used to calculate the continuous opacity contributions from H I, H$^-$, He$^-$, He I, He II bound-free and free-free, H_2^- free-free, Rayleigh scattering of He I, H_2, and H I, and Thompson scattering by e^-. We have also included the Lebedev, Presnyakov, & Sobel'man (2000) H_2^+ free-free and bound-free opacity data. The method used by A. J. Booth & A. E. Lynas-Gray (2002, private communication) for each absorption or scattering process is summarized in Table 2 along with the data for all the other sources of opacity. We have not included any photodissociation processes for HeH$^+$, since these are considered unimportant or important only at extreme-ultraviolet wavelengths (Roberge & Dalgarno 1982). We have also included H I line absorption by using the STARK subroutine from the ATLAS12 (Kurucz 1993) program. H I line absorption is important for temperatures greater than $\sim$7500 K.

In this work we make use of the most recent CIA data, which are in a tabular form. We use the H_2-He CIA data of

Jørgensen et al. (2000), which cover the temperature range of 1000–7000 K and the wavenumber range of 25–20,000 cm^{-1}, the H_2-H_2 data of Borysow, Jørgensen, & Fu (2001), which cover the temperature range of 1000–7000 K and the wavenumber range of 20–20,000 cm^{-1}, and the H-He data of Gustafsson & Frommhold (2001), which cover the temperature range of 1500–10,000 K and the wavenumber range of 50–11,000 cm^{-1}. No CIA data for H-He collisions were available to Lenzuni et al. (1991) and Alexander & Ferguson (1994), but these data have been used by Rohrmann et al. (2002) in the calculation of synthetic white dwarf spectra. Our calculations indicate that at low hydrogen mass fractions, $\log \rho \sim -8$, and $\log T \sim 3.5$, H-He CIA contributes significantly to the Rosseland mean opacity and is the dominant source of continuous opacity between wavelengths of $\sim$3.3 and $\sim$13 μm. We have neglected H-H_2 CIA, however, since it has only a small effect on opacity in a narrow temperature range when H_2 and H are of near equal abundances. At low hydrogen mass fractions, low temperatures, and moderate to high densities, He-He CIA may have an effect on opacity. We have not found any He-He opacity data and so have not been able to include this source of opacity in our calculations.

For the purposes of our calculation, the CIA opacity tables of Jørgensen et al. (2000), Borysow et al. (2001), and Gustafsson & Frommhold (2001) are interpolated using a bicubic spline. Frequencies at which CIA is an important source of opacities are covered by the frequency ranges of the data tables. Beyond the upper temperature limit of the CIA data tables, many opacity sources exceed, by several orders of magnitude, the opacity from CIA. However, CIA from H_2-He and H_2-H_2 collisions remains important for some temperatures below 1000 K. Therefore, the calculation of the total opacity is limited only by the lower temperature limits of the H_2-He and H_2-H_2 CIA data tables, which is 1000 K.

To investigate the effect of direct absorption by H_3^+, the ab initio rotational-vibrational line list of Neale et al. (1996) was used. This line list contains over 3×10^6 lines between 0 and 15,000 cm^{-1}, all of which were used. A thermal Doppler line profile was used to distribute the intensity of each line; this approximation to the true line profile is valid, since all the H_3^+ lines are weak, such that the extended line wings contribute little to the overall opacity. H_3^+ was found to contribute up to 15% of the Rosseland mean opacity via line absorption. This is far smaller than the indirect effect H_3^+ has on opacity through electron donation, which can increase the Rosseland
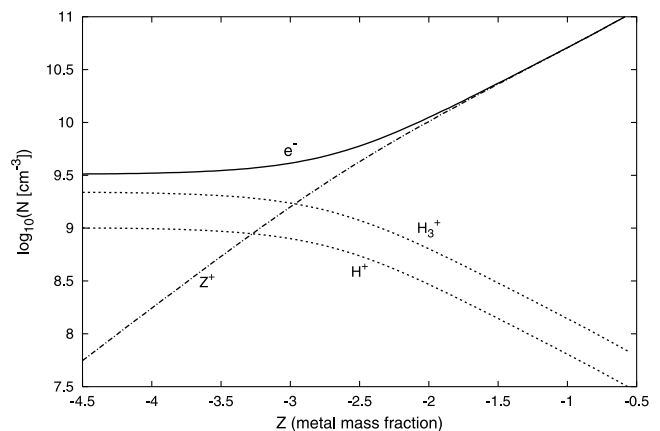

FIG. 5.—Number densities of H_3^+, H^+, e^-, and ionized metals (Z^+) as a function of metal mass fraction, at $T = 3500$ K and $\rho = 10^{-6}$ g cm^{-3}.

TABLE 2

Sources of Continuous Monochromatic Opacity Used in the Calculation, with
Temperature and Wavenumber Limits if Applicable

| | Limits | | |
| | T (K) | Wavenumber (cm⁻¹) | |
Opacity	T (K)	Wavenumber (cm⁻¹)	Reference
H_2-He CIA	1000–7000	25–20000	1
H_2-H_2 CIA	1000–7000	20–20000	2
H-He CIA	1500–10000	50–10000	3
H^- bound-free	...	< 80000	4
H^- free-free	1400–10000	< 55000	4
He^- free-free	660–22000	1400–10000	5
He bound-free	...	...	6
He free-free	...	...	6
He^+ bound-free	...	...	6
He^+ free-free	...	...	6
H bound-free	...	...	7
H free-free	...	...	8
H_2^- free-free	658–28500	>1400–10000	9
H_2^+ bound-free, free-free	4500–10000	2000–46000	10
H_2 Rayleigh scattering	...	>9.76	6
H Rayleigh scattering	...	< 82000	6
He Rayleigh scattering	...	>17.2	6
e^- Thomson scattering	...	...	8
H_3^+ line opacity	...	< 15000	11
H I line opacity	...	...	12

References.—(1) Jørgensen et al. 2000; (2) Borysow et al. 2001; (3) Gustafsson & Frommhold 2001; (4) fits of John 1988; (5) Bell, Berrington, & Croskery 1982; (6) method of Kurucz 1970; (7) method of Gray 1976; (8) method of Gray 1976 using Gaunt factors from Karzas & Latter 1961; (9) Bell 1980; (10) Lebedev et al. 2000; (11) Neale et al. 1996; (12) subroutine from ATLAS 12, Kurucz 1993.

mean opacity by over a factor of 3. However, it implies that H_3^+ lines may well be observable in cool Population III stellar spectra. We have identified a mistake in Figures 1 and 2 of Neale et al. (1996). An incorrect degeneracy factor of 2 instead of 8/3 was used to calculate the absorption by hotter lines in these figures, which resulted in the quoted absorption and emission being reduced by up to 25%. The mistake affects only Figures 1 and 2 and has no bearing on the Einstein A-coefficients of the Neale et al. (1996) line list.

The ion HeH^+ has a strong electric dipole moment and so will have a strong infrared spectrum. We have not been able to find an extensive set of HeH^+ line intensities, so we cannot include HeH^+ line absorption in our opacity calculation. The line opacity of H_3^+ only contributes significantly to the Rosseland mean opacity when the opacity of the gas is low and the number density of H_3^+ is high. The number density of HeH^+ exceeds H_3^+ only at high temperatures, when the Rosseland mean opacity is high. We would expect the total line absorption intensities of HeH^+ per molecule to be weaker than that of H_3^+, so we believe that HeH^+ will have little effect on the opacity, but this needs to be verified.

Figure 6 shows the frequency-dependent opacity of the dominant contributors to the total continuous opacity at $T = 3500$ K, $\rho = 10^{-6}$ g cm^{-3}, and $X = 0.72$. The total opacity is calculated by summing all the contributors to the opacity. This figure illustrates the strength of CIA and H^- and H_3^+ line absorption, hence the importance that these sources of opacity are correctly accounted for. The H_3^+ line absorption has a clear effect on the frequency-dependent opacity between 1500 and 8000 cm^{-1}. This indicates that line absorption may well be observable in certain cool, dense, metal-free stars: brown and possibly cool white dwarfs.

The Rosseland mean opacity is defined by

$$\frac{1}{\kappa_R} = \frac{\int_0^\infty (1/\kappa_\nu)(\partial B_\nu/\partial T)\, d\nu}{\int_0^\infty (\partial B_\nu/\partial T)\, d\nu}, \qquad (4)$$

where B_ν is the Planck function, κ_R is the Rosseland mean opacity, and κ_ν is the monochromatic opacity. The denominator is evaluated analytically, but the numerator must be evaluated numerically. We use 30,000 integration points, which is sufficient to account for H_3^+ line absorption and to converge the integration. The partition functions we have used to calculate the number densities of the various species limit us to temperatures above 1000 K. We therefore only give
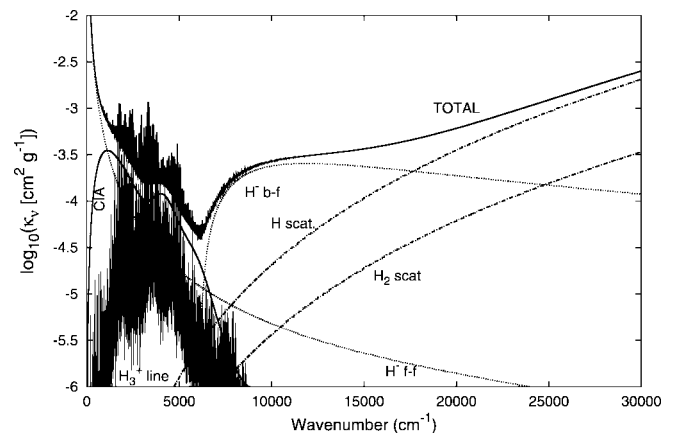

Fig. 6.—Dominant sources of monochromatic opacity as a function of wavenumber, at 3500 K and $\rho = 10^{-6}$ g cm^{-3}.

opacity data for temperatures above 1000 K. This minimum temperature is sufficient for our stellar models.

Figure 7 shows the Rosseland mean opacity calculated in this work along with those of Lenzuni et al. (1991) and Alexander & Ferguson (1994) at $\rho = 10^{-7}$ and $X = 0.72$. The Alexander & Ferguson (1994) data were interpolated using a bicubic spline. A density of $\rho = 10^{-7}$ is too low for the effect of H_3^+ on the number density of H^- to be evident. However, at this density the H_3^+ line opacity is strong enough to contribute 13% of the Rosseland mean opacity at 3250 K. The Rosseland mean opacity of this work for $T < 3500$ K is significantly higher than those of Lenzuni et al. (1991) and Alexander & Ferguson (1994). At these temperatures the opacity is dominated by CIA and a little H_3^+ line opacity. The older works of Lenzuni et al. (1991) and Alexander & Ferguson (1994) do not include H_3^+ line opacity and use older CIA data, which is weaker than the more recent CIA data (see Borysow et al. 2001; Jørgensen et al. 2000). Therefore, a greater opacity at these temperatures is to be expected.

Figure 8 shows a plot of the Rosseland mean opacity at $\rho = 10^{-5}$ g cm^{-3} and $X = 0.72$. The opacities were calculated with the H_3^+ partition functions of Patch (1968), Neale & Tennyson (1995), and Chandra et al. (1991) and also without accounting for H_3^+. The Rosseland mean opacity of Lenzuni et al. (1991) is also plotted, but that of Alexander & Ferguson (1994) does not extend to these high densities. Again, the difference between the opacity of Lenzuni et al. (1991) and that of this work is evident; at these temperatures, CIA is important for $T < 4500$ K and accounts for part of the difference. H_3^+ line absorption is weak, making up $\sim 1.1\%$ of the Rosseland mean opacity at 4000 K, but the most important factor is clearly attributable to the effect of H_3^+ on the opacity. The partition functions of Patch (1968) and Chandra et al. (1991) lead to an underprediction of the abundance of H^- and hence the opacity. It would appear that H_3^+ has an effect on the opacity several times stronger, and to about 500 K hotter, than predicted by the partition functions of Patch (1968) and Chandra et al. (1991). At higher densities still, these differences are even larger, and H_3^+ electron donation becomes even more important. The contribution of H_3^+ line absorption to the Rosseland mean opacity peaks at about $\log \rho = -7.5$ and $T = 3125$ K, at which it is 15% of the opacity.

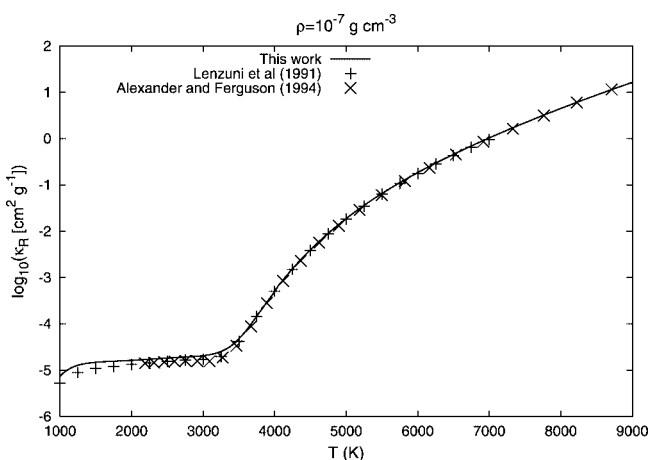We give Rosseland mean opacities for a range of densities, temperatures, and hydrogen mass fractions in Table 3.
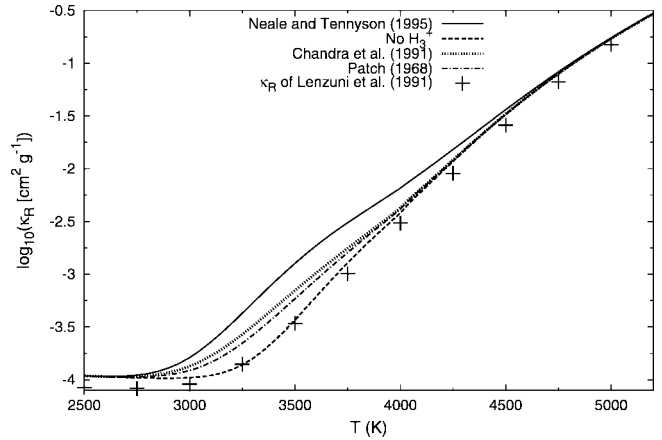

Fig. 8.—Comparison of Rosseland mean opacity at $\rho = 10^{-5}$ calculated with the partition functions of Neale & Tennyson (1995), Chandra et al. (1991), and Patch (1968) and without H_3^+. The Rosseland opacity of Lenzuni et al. (1991) is also plotted.

3. STELLAR EVOLUTION CALCULATIONS

We use the one-dimensional CESAM stellar evolution code (Morel 1997) for our calculations. The CESAM code has been widely applied to helio- and asteroseismology but has also been used for studies of low-mass stars (0.6 $M_\odot$; Morel & Baglin 1999).

The basic input physics is identical to that described by Morel (1997), except for the nuclear reaction rates, opacities, and equations of state, which are as follows: We use the recent NACRE (Angulo et al. 1999) compilation of nuclear reaction rates, which had been previously incorporated into the CESAM code and used for solar evolution models (Morel et al. 1999). The recently improved and extended OPAL equation of state (Rogers & Nayfonov 2002), which we refer to as OPAL02, is used for all temperatures and densities, from the core to the surface of the star. The most recent OPAL opacities (Iglesias & Rogers 1996), which we refer to as OPAL96, are used for temperatures above 9000 K, and the opacity data discussed in § 2 are used for $T < 9000$ K. The equation of state discussed in § 2.1 is used solely to calculate the number densities for use in the calculation of the low-temperature opacities ($T < 9000$ K). The OPAL02 equation of state provides the various thermodynamic quantities necessary for the calculation. To investigate the effects of H_3^+ on these models, we calculate models using two different low-temperature opacity functions. First, we perform a set of calculations using the Neale & Tennyson (1995) H_3^+ partition function, and second, we repeat the calculation while completely neglecting H_3^+.

It should be noted that the OPAL96 opacities are limited to values of $\log R \le 1$, where $R = \rho/(T^3 10^{-18})$. As the mass of a star decreases, its density increases, such that for low-metallicity stars of about 0.7 $M_\odot$ and below, values of $\log R$ exceed 1 and can exceed 2 in a star of 0.4 $M_\odot$. In such circumstances, we have extrapolated the OPAL96 opacity tables to higher values of $\log R$. An extrapolation to $\log R = 2$ requires an extrapolation of an order of magnitude in density or an extrapolation of just over a factor of 2 in temperature. However, the region in which we are forced to extrapolate the OPAL96 opacities corresponds to the convective regions of the stars. Since convective, and not radiative, energy transport is dominant, the extrapolation of the OPAL96 opacities is

Fig. 7.—Comparison of available Rosseland mean opacity for a hydrogen-helium gas, at $\rho = 10^{-7}$ g cm^{-3}.

TABLE 3
Rosseland Mean Opacities (κ_R)

X	$\log_{10}[\rho \ (\mathrm{g \ cm^{-3}})]$	T (K)	$\log_{10}[\kappa_R \ (\mathrm{cm^2 \ g^{-1}})]$
0.70E+00	−5.50E+00	2.00E+03	−4.158E+00
0.70E+00	−5.50E+00	2.25E+03	−4.181E+00
0.70E+00	−5.50E+00	2.50E+03	−4.189E+00
0.70E+00	−5.50E+00	2.75E+03	−4.179E+00
0.70E+00	−5.50E+00	3.00E+03	−4.095E+00
0.70E+00	−5.50E+00	3.25E+03	−3.802E+00
0.70E+00	−5.50E+00	3.50E+03	−3.374E+00
0.70E+00	−5.50E+00	3.75E+03	−2.973E+00
0.70E+00	−5.50E+00	4.00E+03	−2.593E+00
0.70E+00	−5.50E+00	4.25E+03	−2.157E+00
0.70E+00	−5.50E+00	4.50E+03	−1.738E+00
0.70E+00	−5.50E+00	4.75E+03	−1.362E+00
0.70E+00	−5.50E+00	5.00E+03	−1.031E+00
0.70E+00	−5.50E+00	5.25E+03	−7.399E−01
0.70E+00	−5.50E+00	5.50E+03	−4.811E−01
0.70E+00	−5.50E+00	5.75E+03	−2.486E−01
0.70E+00	−5.50E+00	6.00E+03	−3.780E−02
0.70E+00	−5.50E+00	6.25E+03	1.552E−01
0.70E+00	−5.50E+00	6.50E+03	3.335E−01
0.70E+00	−5.50E+00	6.75E+03	4.994E−01
0.70E+00	−5.50E+00	7.00E+03	6.551E−01

Notes.—The opacities are for a range of hydrogen mass fractions ($0 \leq X \leq 1$), densities ($10^{-14} \leq \log_{10}[\rho \ (\mathrm{g \ cm^{-3}})] \leq 10^{-2}$), and temperatures [$1000 \leq T$ (K) ≤ 9000]. Table 3 is published in its entirety in the electronic edition of the *Astrophysical Journal*. A portion is shown here for guidance regarding its form and content.

unimportant. To test that this extrapolation is unimportant, we perturbed the extrapolated OPAL96 opacity by multiplying by $\log R$ when $\log R \geq 1$. We found that the calculations performed with and without this opacity perturbation were identical.

The minimum mass of the star that we study is imposed by the boundaries of the OPAL02 equation-of-state tables. These equation-of-state tables do not cover all the temperatures and densities within our model stars of mass less than about $0.15 \ M_\odot$. Hence, we limit our calculation to masses of $0.15 \ M_\odot$ and above.

A gray atmosphere is used for the surface boundary condition, and the temperature stratification follows a $T(\tau)$ relationship based on Hopf's law. A thorough discussion of this and other model atmospheres used in CESAM can be found in Morel et al. (1994). In the zero-metallicity model atmospheres of Saumon et al. (1994), significant differences between the gray and nongray [$\log (g) = 5$] model atmospheres do occur for $T_\mathrm{eff} < 4500$ K. Consequently, for stars below this T_eff, gray atmospheres give relatively poor boundary conditions. Nongray atmospheres effectively increase the average atmospheric opacity relative to the gray case (Saumon et al. 1994). In this work the inadequacies of the gray atmosphere are relatively unimportant, because this is primarily a differential study in which we seek to show that the use of the H$_3^+$ partition function of Neale & Tennyson (1995) causes H$_3^+$ to have a greater effect on stellar evolution than previously thought. To enable us to calculate more realistic evolutionary models, we are in the process of calculating nongray atmospheres for zero-metallicity, very low mass stars.

The initial conditions for our calculation are those of a collapsing pre–main-sequence star at the top of the Hayashi track, as described in Morel (1997). Briefly, the pre–main-sequence star is in quasi-static equilibrium, and energy is released only through gravitational collapse. The star is fully convective, so that entropy is constant throughout the star. The initial conditions are described by a contraction constant c. For a $1 \ M_\odot$ star, Morel (1997) suggests a contraction constant of $0.02 \ L_\odot \ M_\odot^{-1} \ \mathrm{K}^{-1}$. In this work we use a constant value of $0.015 \ L_\odot \ M_\odot^{-1} \ \mathrm{K}^{-1}$. We find that the value of the contraction constant has only a small effect on the position of the resulting star on the main sequence.

Our models are computed without mass loss and rotation. We follow Marigo et al. (2001) and use an initial hydrogen mass fraction of $X = 0.77$. We set the metal mass fraction to be $Z = 10^{-14}$. This is low enough to make the effect of metals negligible, while avoiding numerical problems with extremely low and zero values of Z. This leaves a helium mass fraction (Y) of marginally under 0.23.

4. RESULTS AND DISCUSSION

Figure 9 shows the evolution paths of zero-metallicity model stars between 0.4 and $0.15 \ M_\odot$ calculated with and without the effects of H$_3^+$. Symbols are placed on the curves when the core hydrogen mass fractions are 10^{-2}, 10^{-3}, and 10^{-4}. Initially, the pre–main-sequence stars of $0.4 \ M_\odot$ and less, with and without H$_3^+$, contract along identical paths; the density within the atmosphere at this stage is too low for H$_3^+$ to have any effect. As the star becomes more dense and before the stars reach the main sequence, the paths separate as H$_3^+$ starts to become the dominant positive ion within the atmosphere. At zero-age main sequence, the star with H$_3^+$ has a lower T_eff and luminosity than the star in which H$_3^+$ is not accounted for. This trend continues throughout the main-sequence lifetime of the stars. For stars with higher masses of 0.5 and $0.45 \ M_\odot$, we find that H$_3^+$ affects the late pre–main-sequence and early main-sequence evolution but that the evolutionary tracks on the main sequence converge as the star
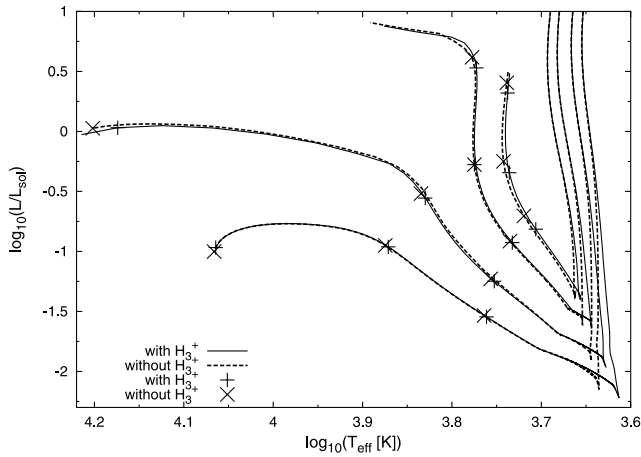
FIG. 9.—Evolutionary tracks of 0.4, 0.3, 0.2, and 0.15 $M_\odot$ zero-metallicity stars calculated by both neglecting and including the effect of H_3^+ on opacity. Symbols are placed at values of the hydrogen mass fraction of 10^{-2}, 10^{-3}, and 10^{-4} at the center of the star.

becomes hotter in the late main sequence, and H_3^+ is destroyed. Our evolution tracks are in agreement with the zero-metallicity calculations of Marigo et al. (2001), which cover masses greater than 0.7 $M_\odot$, and also of Siess et al. (2002), which cover masses greater than 0.8 $M_\odot$.

This tendency for model stars of less than 0.5 $M_\odot$ with H_3^+ to have lower $T_{\rm eff}$ and luminosity than their counterparts without H_3^+ is shown again in Figure 10. This figure shows the 14 Gyr isochrone for model stars calculated with and without the effects of H_3^+, with symbols placed at intervals of 0.05 $M_\odot$. The three curves represent models calculated using the Neale & Tennyson (1995) H_3^+ partition function and the Chandra et al. (1991) H_3^+ partition function, also neglecting H_3^+. For 14 Gyr old stars of 0.15 $M_\odot$, the difference in $T_{\rm eff}$ between models calculated with the Neale & Tennyson (1995) partition function and those in which H_3^+ is neglected is over 200 K, and the difference in luminosity is about 18%. The models calculated with the Neale & Tennyson (1995) partition function show that H_3^+ has a significantly greater effect, which extends to higher masses, than that predicted by models calculated with the Chandra et al. (1991) partition function. This
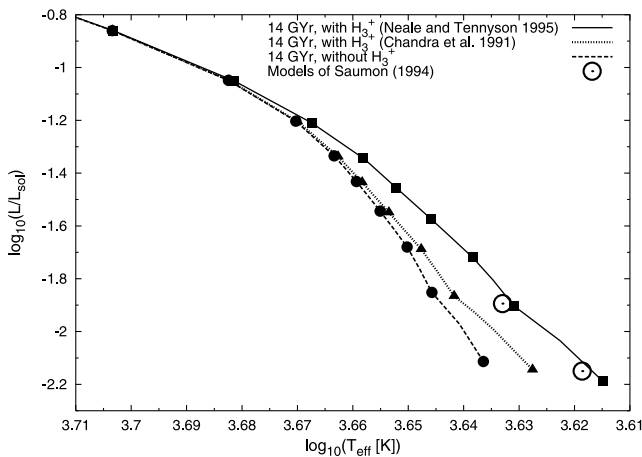
illustrates the importance of using the Neale & Tennyson (1995) partition function in low-mass evolution models. The luminosity and effective temperature of the 0.2 and 0.15 $M_\odot$ zero-metallicity main-sequence model stars of Saumon et al. (1994) are also plotted in Figure 10. Since Saumon et al. (1994) used the Chandra et al. (1991) partition function, their results would have been expected to lie on the isochrone calculated with the Chandra et al. (1991) partition function. However, the models of Saumon et al. (1994) lie closer to the isochrone calculated with the Neale & Tennyson (1995) partition function. Saumon et al. (1994) used nongray atmospheres, whereas in this work we have used gray atmospheres, so the reason for this difference is likely to be due to the breakdown of the gray approximation in very low mass stars. Saumon et al. (1994) commented that using nongray models effectively increases the atmospheric opacity over gray model atmospheres. Hence, nongray stars have a lower $T_{\rm eff}$ than their gray counterparts.

It is clear from Figure 10 that the strength of the effect of H_3^+ increases with decreasing mass. As long as H^- remains the dominant source of opacity, the strength of the effect of H_3^+ will continue to increase with decreasing mass. The effect of H_3^+ within the atmosphere will diminish when CIA becomes the dominant source of opacity, at about $T_{\rm eff} < 3000$ K. However, in a shell below the photospheres of such stars, hotter, denser gas exists in which H^- remains the dominant source of opacity, and H_3^+ will again affect opacity.

Figure 11 shows the evolution of the central temperature for model stars of mass 0.8, 0.6, 0.4, 0.25, and 0.15 $M_\odot$, calculated with and without the effects of H_3^+. Again, it is seen that H_3^+ has no effect on the central temperatures of model stars of mass 0.6 $M_\odot$ and above. For the model stars of 0.25 and 0.15 $M_\odot$, the increased atmospheric opacity due to H_3^+ acts to reduce the central temperature. This in turn reduces the nuclear reaction rates and so increases the hydrogen-burning lifetime of the model star. H_3^+ also acts to reduce the pre–main-sequence and early main-sequence central temperatures of the 0.4 $M_\odot$ model. However, for most of the main sequence, the central temperature of the 0.4 $M_\odot$ model star that neglects H_3^+ is cooler than the 0.4 $M_\odot$ model that accounts for H_3^+. This results in a longer hydrogen-burning lifetime for the model that neglects H_3^+. The reason for this is that the
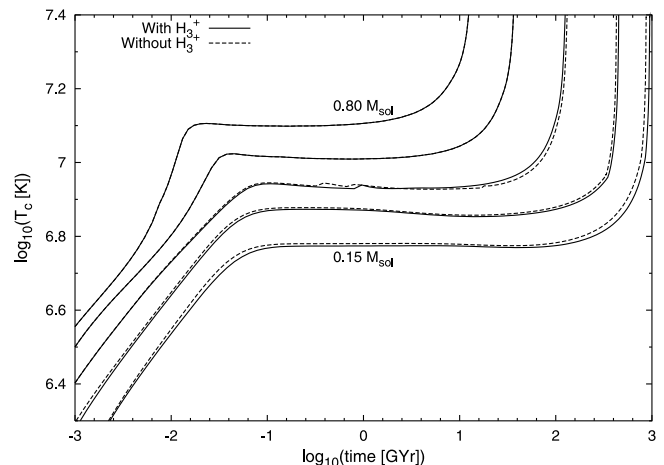

FIG. 10.—The 14 Gyr isochrone for zero-metallicity stars of mass 0.55–0.15 $M_\odot$. Symbols are placed between masses of 0.55 and 0.15 $M_\odot$ in steps of 0.05 $M_\odot$. Also shown are the 0.2 and 0.15 $M_\odot$, zero-metallicity, main-sequence models of Saumon et al. (1994).

FIG. 11.—Central temperature as a function of time for stars of masses 0.8, 0.6, 0.4, 0.25, and 0.15 $M_\odot$. Curves are shown both including and neglecting H_3^+.

$0.4\ M_\odot$ model star without H_3^+ has a fully convective interior at zero-age main sequence, whereas the $0.4\ M_\odot$ model star that accounts for H_3^+ starts zero-age main sequence with a radiative interior. Convective mixing in a fully convective star makes the hydrogen throughout the star available for fusion in the core. Conversely, in a star with a radiative interior, there is only very limited mixing of material, so that only the hydrogen in the core is available for fusion. Hence, the convective model star without H_3^+ has a longer lifetime than the radiative model star with H_3^+, even though the former is more luminous. It appears that H_3^+ within the atmosphere can have an effect on the structure and energy transport mechanisms within these low-mass stars that have interior temperature gradients close to the adiabatic temperature gradient. Therefore, slight changes in the temperature gradient brought about by increased atmospheric opacity can change the main energy transport method. All the stars of mass less than $0.4\ M_\odot$ have a fully convective interior at zero-age main sequence, and all of the stars develop a radiative interior at some point later in their main-sequence evolution. After developing a radiative interior, the rate of evolution of the star along the main sequence increases dramatically.

5. CONCLUSION

We have calculated new low-temperature, zero-metallicity Rosseland mean opacities using the latest collision-induced absorption opacity data and the latest H_3^+ partition function and line opacity data. The results of this calculation confirm that at high densities and intermediate temperatures, H_3^+ becomes the dominant positive ion. Furthermore, using the H_3^+ Neale & Tennyson (1995) partition function instead of an older partition function causes the temperature and density ranges at which H_3^+ forms to expand, as well as increasing its abundance by up to an order of magnitude. This in turn increases the abundance of electrons, and hence H^- and other negative ions, therefore affecting the opacity of the gas by a greater degree than was previously thought. The H_3^+ line opacity at certain temperatures and densities can contribute up to 15% of the Rosseland mean opacity. H_3^+ lines may well be observable within cool Population III stars, and all models of such stars should account for direct absorption by H_3^+.

The new Rosseland mean opacities have been included in evolution models of very low mass, zero-metallicity stars, enabling us to investigate the effect of H_3^+ on the evolution of these stars. For late pre–main-sequence and early main-sequence stars of mass less than $0.55\ M_\odot$, we find that H_3^+ can cause the atmosphere to cool and the star to drop slightly in luminosity. For stars of $0.45\ M_\odot$ and below, this effect becomes strong enough to affect the main-sequence structure and lifetime of the star.

The results presented here show that as the mass of a zero-metallicity star is reduced, the effect of H_3^+ on its evolution, structure, luminosity, and temperature increase. Since the Neale & Tennyson (1995) partition function is much larger than the partition function of Chandra et al. (1991), used by Saumon et al. (1994), its corresponding effect on opacity is larger. Hence, if the effect of H_3^+ continues to grow in objects of below $0.15\ M_\odot$, then H_3^+ will effect the evolution of zero-metallicity, very low mass stars and brown dwarfs to a greater extent than previously believed.

REFERENCES

Alexander, D. R., & Ferguson J. W. 1994, ApJ, 437, 879
Allard, F., Hauschildt, P. H., Alexander, D. R., Tamanai, A., & Schweitzer, A. 2001, ApJ, 556, 357
Angulo, C., et al. 1999, Nucl. Phys. A, 656, 3
Baraffe, I., Chabrier, G., Allard, F., & Hauschildt, P. H. 1997, A&A, 327, 1054
———. 1998, A&A, 337, 403
———. 2002, A&A, 382, 563
Bell, K. L. 1980, J. Phys. B, 13, 1859
Bell, K. L., Berrington, K. A., & Croskery, J. P. 1982, J. Phys. B, 15, 977
Bergeron, P., Ruiz, M. T., & Leggett, S. K. 1997, ApJS, 108, 339
Bergeron, P., Saumon, D., & Wesemael, F. 1995, ApJ, 443, 764
Borysow, A., Jørgensen, U. G., & Fu, Y. 2001, J. Quant. Spectrosc. Radiat. Transfer, 68, 235
Chabrier, G., & Baraffe, I. 1997, A&A, 327, 1039
Chandra, S., Gaur, V. P., & Pande, M. C. 1991, J. Quant. Spectrosc. Radiat. Transfer, 45, 57
Christlieb, N., et al. 2002, Nature, 419, 904
de Araújo, J. C. N., & Opher, R. 1989, MNRAS, 239, 371
Gray, D. F. 1976, The Observation and Analysis of Stellar Photospheres (New York: Wiley)
Grevesse, N., & Sauval, A. J. 1998, Space Sci. Rev., 85, 161
Gustafsson, M., & Frommhold, L. 2001, ApJ, 546, 1168
Hauschildt, P. H., Allard, F., & Baron, E. 1999, ApJ, 512, 377
Herbst, E. 2000, Philos. Trans. R. Soc. London A, 358, 2523
Iglesias, C. A., & Rogers, F. R. 1996, ApJ, 464, 943
John, T. L. 1988, A&A, 193, 189
Jørgensen, U. G., Hammer, D., Borysow, A., & Falkesgaard, J. 2000, A&A, 361, 283

Karzas, W. J., & Latter, R. 1961, ApJS, 6, 167
Kashlinsky, A., & Rees, M. J. 1983, MNRAS, 205, 955
Kurucz, R. L. 1970, SAO Spec. Rep. 308 (Cambridge: SAO)
———. 1993, in IAU Colloq. 138, Peculiar versus Normal Phenomena in A-Type and Related Stars, ed. M. M. Dworetsky, F. Castelli, & R. Faraggiana (ASP Conf. Ser. 44; San Francisco: ASP), 87
Lebedev, V. S., Presnyakov, L. P., & Sobel'man, I. I. 2000, Astron. Rep., 44, 338
Lenzuni, P., Chernoff, F. P., & Salpeter, E. E. 1991, ApJS, 76, 759
Marigo, P., Girardi, L., Chiosi, C., & Wood, P. R. 2001, A&A, 371, 152
Mihalas, D., Däppen, W., & Hummer, D. G. 1988, ApJ, 331, 815
Morel, P. 1997, A&AS, 124, 597
Morel, P., & Baglin, A. 1999, A&A, 345, 156
Morel, P., Pichon, B., Provost, J., & Berthomieu, G. 1999, A&A, 350, 275
Morel, P., van't Veer, C., Provost, J., Berthomieu, G., Castelli, F., Cayrel, R., Goupil, M. J., & Lebreton, Y. 1994, A&A, 286, 91
Nakamura, F., & Umemura, M. 2001, ApJ, 548, 19
Neale, L., Miller, S., & Tennyson, J. 1996, ApJ, 464, 516
Neale, L., & Tennyson, J. 1995, ApJ, 454, L169
Patch, R. W. 1968, J. Chem. Phys., 49, 961
Proffitt, C. R. 1994, ApJ, 425, 849
Richard, O., Michaud, G., Richer, J., Turcotte, S., Turck-Chièze, S., & VandenBerg, D. A. 2002, ApJ, 568, 979
Roberge, W., & Dalgarno, A. 1982, ApJ, 255, 489
Rogers, F. J., & Nayfonov, A. 2002, ApJ, 576, 1064
Rohrmann, R. D. 2001, MNRAS, 323, 699
Rohrmann, R. D., Serenelli, A. M., Althaus, L. G., & Benvenuto, O. G. 2002, MNRAS, 335, 499

Saumon, D., Bergeron, P., Lunine, J. I., Hubbard, W. B., & Burrows, A. 1994, ApJ, 424, 333

Saumon, D., & Jacobson, S. B. 1999, ApJ, 511, L107

Sauval, A. J., & Tatum, J. B. 1984, ApJS, 56, 193

Siess, L., Livio, M., & Lattanzio, J. 2002, ApJ, 570, 329

Stancil, P. C. 1994, J. Quant. Spectrosc. Radiat. Transfer, 55, 849

Tohline, J. E. 1980, ApJ, 239, 417

Turcotte, S., Richer, J., Michaud, G., Iglesias, C. A., & Rogers, F. J. 1998, ApJ, 504, 539

Umeda, H., & Nomoto, K. 2003, Nature, 422, 871

VandenBerg, D. A., Swenson, F. J., Rogers, F. R., Iglesias, A., & Alexander, D. R. 2000, ApJ, 532, 430